PERGAMON

Atmospheric Environment 37 (2003) 2193–2205

ATMOSPHERIC ENVIRONMENT

www.elsevier.com/locate/atmosenv

Atmospheric lifetime as a probe of radical chemistry in the boundary layer

Nadine Bell[a,*,1], Dwayne E. Heard[a], Michael J. Pilling[a], Alison S. Tomlin[b]

[a] *School of Chemistry, University of Leeds, Leeds, LS2 9JT, UK*
[b] *Department of Fuel and Energy, University of Leeds, Leeds, LS2 9JT, UK*

Received 8 May 2002; received in revised form 3 December 2002; accepted 17 February 2003

Abstract

Determination of the atmospheric lifetime of radical species provides a potentially powerful method to resolve discrepancies between their modelled and measured concentrations. Theoretical perturbation analysis is employed to investigate the relationship between atmospheric lifetime (τ) and decay time (λ^{-1}) following concentration perturbation for OH and HO_2 using a model system with constrained NO_x. It is shown that feedback from HO_2 to OH can lead to a non-equivalence of (τ) and (λ^{-1}), depending on the size of the feedback term and the difference in the atmospheric lifetimes of the coupled species. The ideas are applied and extended in a discussion of atmospheric field data from the EASE96 campaign at a remote coastal site. Dynamic information about the relaxation modes and species couplings, available from the eigenvector elements, is investigated for the systems studied. In general, the results suggest that the assignment of a specific decay time to OH is feasible for background boundary layer tropospheric conditions. However, complex couplings between peroxy species lead to non-separable time scales for these species. The relevance of results for the development of a field instrument to measure OH lifetime is discussed.
© 2003 Elsevier Science Ltd. All rights reserved.

Keywords: Photochemistry; Hydrogen oxides; Chemical lifetimes; Perturbation analysis; Eigenmodes

1. Introduction

Following the development of techniques for atmospheric OH radical detection (Crosley, 1995), several field experiments have been carried out to study OH photochemistry in the troposphere (Eisele et al., 1994; Atlas and Ridley, 1996; Mount and Williams, 1997). The field studies have often provided a platform for in situ intercomparison of OH radical measurement techniques. The principal strategy employed to understand the chemistry has so far been comparison of the measured [OH] data with the results of zero-dimensional model [OH] simulations, highly constrained to the observed field data for longer-lived species. The use of a zero-dimensional model with no spatial resolution is presumed adequate for the [OH] model comparison with observed [OH], since transport of such short-lived radical species does not contribute significantly to their local concentration. The experimental data for [OH] must, however, be accompanied by supporting measurements of the longer-lived co-reactant concentrations, photolysis rates, and temperature in the same air mass for a meaningful comparison.

Recent field campaigns designed to characterise the OH radical in the troposphere have observed significant discrepancies between measured and modelled data for [OH] (Eisele et al., 1994, 1996; McKeen et al., 1997; Carslaw et al., 1999a; George et al., 1999). Typically, in both clean and polluted conditions, [OH] is over-predicted by about 50%. An important illustrative

*Corresponding author. Fax: 1-212-6785552.
E-mail address: nbell@giss.nasa.gov (N. Bell).
[1] Present address: NASA Goddard Institute for Space Studies and Center for Climate Research, Columbia University, New York, USA.

1352-2310/03/$ - see front matter © 2003 Elsevier Science Ltd. All rights reserved.
doi:10.1016/S1352-2310(03)00157-2

example is provided by the Fritz Peak Tropospheric OH Photochemistry Experiment 1993, carried out at the Fritz Peak and Idaho Hill Sites in the Rocky Mountains of Colorado, which consisted of an extensive study of a very broad range of trace species and included measurements of [OH] (Mount and Williams, 1997). There was a factor of two discrepancy between field measurement and model prediction of [OH], when the model was constrained by field measurements of concentrations of a wide range of species, including non-methane hydrocarbons (NMHC) (McKeen et al., 1997). The discrepancy was ascribed to an undetermined OH sink, probably a C_{10} terpene, which did not lead to feed back to OH via HO_2.

One possible way to help resolve discrepancies in measured and modelled data is to carry out a different type of measurement which utilises the dynamics of the tropospheric photochemistry. The rate of change of concentration in a spatially homogeneous reaction system is described by a set of ordinary differential equations (ODEs), constrained by initial values:

$$\frac{d\mathbf{c}}{dt} = \mathbf{f}(\mathbf{c}, \mathbf{k}), \quad \mathbf{c}(0) = \mathbf{c}_0, \tag{1}$$

where $\mathbf{f}$ is a vector-valued rate function depending on $\mathbf{c}$, the concentration vector, and $\mathbf{k}$, the vector of reaction rate coefficients. The initial concentrations are represented by the vector $\mathbf{c}_0$.

For a single species, such as OH, Eq. (1) can be expressed in the form

$$\frac{d[OH]}{dt} = P - L, \tag{2}$$

where P and L are the time-dependent rates of production and loss of OH, respectively. A quasi steady state for OH is established within seconds in the troposphere and under these conditions, $P = L$. Model/measurement comparisons are based on Eq. (2) or its steady state equivalent, or on a larger chemistry and transport model involving equivalent chemical rates of change. The production rate, P, includes, for example, contributions from ozone photolysis, HO_2 reaction with NO and, under some conditions, reaction of ozone with alkenes. All of the reactions contributing significantly to $L(t)$ are first order in OH, so that

$$L(t) = \sum_j k_j x_i [OH], \tag{3}$$

where x_i is the concentration of co-reactant X_i and k_j is the bimolecular rate coefficient for reaction between X_i and OH. Thus the rates of production and loss rely on complementary measurements of photolysis rates and of concentrations of a wide range of species. The loss rate, L, is frequently dominated by reactions with NMHC and it is often difficult to ensure that all species have been detected and measured; this problem is particularly severe when a wide range of biogenic or anthropogenic NMHC are present and is illustrated by the model/measurement discrepancy reported by McKeen et al. (1997). The analytical challenge involved in the quantification of mixtures of higher hydrocarbons found in urban areas is clearly demonstrated by the two-dimensional chromatography measurements of Lewis et al. (2000). There is a clear need for further constraints on model/measurement comparisons for OH, if the difficulties experienced at Fritz Peak and elsewhere are to be resolved, or the source of the discrepancy identified.

The atmospheric chemical lifetime (τ) of a species is the reciprocal of its overall local pseudo first-order rate coefficient. For OH

$$\tau_{OH} = \frac{1}{\sum k_j x_i}. \tag{4}$$

Since many of the co-reactant concentrations vary with time, τ_{OH} is time dependent. Combining Eqs. (2)–(4), and setting the time derivative to zero, gives

$$[OH] = P\tau. \tag{5}$$

Thus, the measurement of the OH atmospheric lifetime provides an extra constraint in model/measurement comparison. In particular, it allows explicit recognition of situations where the full range of co-reactants, X_i, has not been fully characterised.

Experimental methods for the determination of the OH atmospheric lifetime via a perturbation technique are currently under development (Kovacs and Brune, 1999; Calpini et al., 1999; Smith and Crosley, 1999). The experiment generally involves photolytic production of OH at mixing ratios above ambient, followed by time-dependent measurement of the concentration as it relaxes. For example, the fluorescence assay by gas expansion (FAGE) technique (Hard et al., 1984) is currently being adapted to provide a measurement of the atmospheric lifetime of OH. Air is drawn into a flow tube, [OH] is enhanced by photolysis of water vapour at 185 nm and monitored with laser induced fluorescence. An [OH] decay profile is then achieved by sequential movement of the photolysis lamp along the flow tube to change the time between generation and detection and the relaxation time determined. The relaxation of the concentrations of reacting chemical species, following a concentration perturbation of this type, are considered in the following sections.

In Section 2, we summarise the response of a system of reactively coupled species to a perturbation, showing that the system relaxes on a sequence of timescales. Provided the perturbation is small so that the Jacobian matrix, $\mathbf{J}$ ($\mathbf{J} = \partial\mathbf{f}/\partial\mathbf{c}$ with elements $J_{ij} = \partial f_j/\partial c_i$), for the system is almost constant during the relaxation, then the system relaxes through a series of exponentials whose reciprocal time constants are the eigenvalues of the Jacobian. The relationship between the chemical lifetime of a species and the eigenvalue(s) is outlined in

Section 3. This relationship is examined in Sections 4 and 5 for OH and HO_2 in the tropospheric boundary layer using a simple linearized tropospheric model. The ideas are then applied and extended in Section 5 in a discussion of atmospheric field data from the EASE96 campaign at Mace Head on the West Coast of Ireland. A discussion of findings is presented in Section 6.

2. Methodology

The response of a nonlinear system of ordinary differential equations to perturbation of one or more of the variables is well documented (Gray and Scott, 1991). Laboratory kineticists use the approach to deal with interfering reactions (Hughes et al., 1992) and the technique finds a general use in the analysis and interpretation of biogeochemical cycles (Lasaga, 1981; Lasaga and Berner, 1998; Chameides and Perdue, 1997).

The system of Eqs. (1) is disturbed at a steady-state solution with a small perturbation $\Delta\mathbf{c}$. To first order, the decay of the perturbation can be expressed by the first term of a Taylor series expansion

$$\frac{(\mathrm{d}\Delta\mathbf{c})}{\mathrm{d}t} = \mathbf{J}\Delta\mathbf{c}. \tag{6}$$

The solution to such a set of linear equations can be written as

$$\Delta\mathbf{c}(t) = \mathbf{U}\mathrm{e}^{\Lambda t}\mathbf{U}^{-1}\Delta\mathbf{c}_0, \quad \Lambda = \mathrm{diag}(\lambda_1, \ldots, \lambda_n). \tag{7}$$

The exponents λ are the eigenvalues of the Jacobian matrix, $\mathbf{J}$. $\mathbf{U}$ is a matrix of right eigenvectors and $\mathbf{U}^{-1}$ is a transpose matrix of left eigenvectors. $\mathbf{U}^{-1}$ can also be thought of as the inverse matrix of $\mathbf{U}$, i.e. $\mathbf{U}\mathbf{U}^{-1} = \mathbf{I}$ where $\mathbf{I}$ is the identity matrix containing diagonal elements equal to 1 with all other elements equal to zero. It can, therefore, be found by either calculating the inverse of the matrix right eigenvectors $\mathbf{U}$, or by computing the left eigenvectors and transposing the matrix, i.e. swapping rows and columns.

For a single component of the system,

$$\Delta c_i(t) = \sum_j \sum_k u_{ij}\mathrm{e}^{\lambda_j t}u_{jk}^{-1}\Delta c_k(0), \tag{8}$$

where u_{ij} is the right eigenvector (for the ith species and jth eigenvalue) and u_{jk}^{-1} is the transpose left eigenvector (for the jth eigenvalue and kth species).

The eigenvalues define the time-scales of the system's response to a small chemical perturbation. Each eigenvalue of the Jacobian matrix is associated with a different time-scale of the locally linear solution of the full equations. The largest negative eigenvalue corresponds to a perturbation that decays very quickly and is associated with the fastest time-scale.

The eigenvectors give information about species coupling and the extent of deviation of $\mathbf{J}$ from a diagonal matrix. If the matrix of eigenvectors has off-diagonal terms then cross couplings occur. It is useful to define a set of modes, $\Delta\mathbf{z}$, where

$$\Delta\mathbf{z} = \mathbf{U}^{-1}\Delta\mathbf{c}(t). \tag{9}$$

Multiplying Eq. (7) on both sides by $\mathbf{U}^{-1}$ and substituting with Eq. (9) leaves

$$\Delta\mathbf{z} = \mathrm{e}^{\Lambda t}\mathbf{U}^{-1}\Delta\mathbf{c}_0. \tag{10}$$

The initial perturbation to the modes is given by

$$\Delta\mathbf{z}_0 = \mathbf{U}^{-1}\Delta\mathbf{c}_0. \tag{11}$$

Thus each mode is related to the initial perturbation by a single eigenvalue and

$$\Delta\mathbf{z}(t) = \mathrm{e}^{\Lambda t}\Delta\mathbf{z}_0. \tag{12}$$

Independent of the choice of the initial $\Delta\mathbf{c}_0$, the linear combination of perturbations has a common time dependence for a specific mode. The perturbation in the modes $\Delta\mathbf{z}$ is related to the perturbation on the species' concentration, $\mathbf{c}(t)$, as given by Eq. (9), and therefore

$$\Delta\mathbf{c}(t) = \mathbf{U}\Delta\mathbf{z}(t). \tag{13}$$

The transpose matrix of the left eigenvectors, $\mathbf{U}^{-1}$, can be thought of as a linear transformation from species into modes. Thus, the eigenvector elements of this matrix give the contribution of each species to each different time-scale. The right eigenvectors, $\mathbf{U}$, can be seen as the inverse transformation matrix. The right eigenvector elements describe the contribution of each eigenmode, relating to an individual timescale, to each species. A full description of the analysis is found in Tomlin et al. (2001).

Such a perturbation analysis is usually applied to a fixed point, for example to establish the stability of a steady state in a dynamical system. Useful information can be derived from the analysis for a time-dependent system provided the concentrations of species involved in the major rate processes do not change significantly over the time-scale of the relaxation of the perturbed species. For such systems the analysis can be considered as studying the perturbation from a "slow manifold" which exists in the full species phase space but is of a lower dimension. Fast processes can be thought of as those relaxing quickly onto the slow manifold and relate to large negative eigenvalues. Slow processes can be considered as dynamically moving within the manifold and relate to small eigenvalues. As long as time-scale separation exists between the perturbed variables and the non-perturbed variables then a linear perturbation analysis can provide a useful interpretation of relaxation processes. For a full explanation of slow manifolds in atmospheric systems see Tomlin et al. (2001). Many of the elements of $\mathbf{J}$ depend explicity on concentration and it is necessary to assume that they and hence $\mathbf{J}$ remain

approximately constant over the timescale of the relaxation of the perturbed species under consideration. The effects of varying concentrations are addressed in more detail in Tomlin et al. (2001) and in the present paper in Sections 4 and 5, with particular reference to OH and peroxy radicals.

3. Relationship between eigenvalue and lifetime

The reciprocal of the chemical lifetime, τ, of a species is equal to the sum of the pseudo-first-order rate coefficients for its removal. The Jacobian matrix allows us to generalise the *local lifetime* (lifetime defined at a specific point in the evolution of the system where the concentrations of the reactants are changing) as

$$\tau_i = -\frac{1}{J_{ii}}. \tag{14}$$

The concentration vector in the rate equations may be ordered according to the lifetimes of the species. If there is no coupling from species with longer lifetimes then the Jacobian is triangular and the eigenvalues equal the diagonal elements, $\lambda_i = J_{ii}$. Hence, the relaxation time following a small perturbation gives directly the chemical lifetime, $\lambda_i = -(\tau_i)^{-1}$ (Turanyi et al., 1993). When $\lambda_i \neq J_{ii}$, the relaxation behaviour may provide novel insights into reaction couplings in the tropospheric chemical mechanism.

The methodology may prove to be of use in designing experiments for determining the dynamics of reaction pathways. In systems where component species are not well identified or elementary reaction sequences are not well understood, studying the response to perturbations may give an indication of the mechanisms of reaction pathways which is not available, or would be time consuming to obtain, by conventional means. Such information is explored in the correlation metric construction for enzymatic systems (Arkin et al., 1997) where random perturbations are applied to input species concentrations and the response of other species is measured on varying time-scales and presented as a series of time delays. The correlations between the species concentrations and the time delays of the species response not only demonstrate which species are coupled, but also provide information on the time dependence of the reaction sequence.

The concept of decay times in atmospheric chemistry that differ from atmospheric chemical lifetimes is not new. Previous studies have examined chemical perturbations to global systems including perturbations to the natural CH_4–CO–OH cycle, which is very strongly coupled and plays a crucial role in the self-cleansing processes in the troposphere (Prather, 1994, 1996). It was found that for the CH_4–CO–OH cycle the longest time constant (smallest absolute eigenvalue) always exceeds the lifetime defined by the steady-state loss frequency for CH_4, the longest-lived gas. Prather (1998) showed how photolytic coupling between O_3 and N_2O in the N_2O–NO_y–O_3 system causes more rapid decay of the longest-lived mode, decay of N_2O, than expected based on the atmospheric lifetime of N_2O, which has implications for the inference of anthropogenic source strengths. Poppe (1999) has examined the response of a model tropospheric chemical system to perturbation, through a locally linear analysis. The present paper primarily addresses the feasibility of measuring the chemical lifetime of OH in field experiments, using a perturbation technique. Its emphasis is, therefore, a study of the relationship between eigenvalues and chemical lifetimes, which is introduced in the following section.

4. Linearized model system of fast photochemistry

In this section, a simplified model system, which describes the oxidation of CO in the boundary layer and captures the main features of the tropospheric HO_x ($HO_x = OH + HO_2$) cycle, is used to examine the relationship between eigenvalues (λ_i) and lifetimes (τ_i) for OH and HO_2. It is assumed that the air mass is well mixed and not affected by transport on the time-scales of this analysis, allowing a zero-dimensional box model to be used.

The reaction scheme is as follows:

$$\text{(R1a)}\ O(^1D) + H_2O \xrightarrow{k_{1a}} 2OH,$$

$$\text{(R1b)}\ O(^1D) + N_2 \xrightarrow{k_{1b}}$$

$$\text{(R1c)}\ O(^1D) + O_2 \xrightarrow{k_{1c}}$$

$$\text{(R2)}\ OH + CO \xrightarrow{k_2} HO_2 + \text{products},$$

$$\text{(R3)}\ HO_2 + NO \xrightarrow{k_3} OH + NO_2,$$

$$\text{(R4)}\ OH + NO_2 \xrightarrow{k_4} HNO_3,$$

$$\text{(R5)}\ HO_2 + HO_2 \xrightarrow{k_5} H_2O_2 + O_2.$$

The rate coefficients and model conditions are shown in Table 1. For the purpose of this study we neglect the $OH + HO_2$ reaction to facilitate analytical calculation of the eigenvalues. Moreover, the reaction has been shown to be unimportant for OH and HO_2 loss in the boundary layer air (Carslaw et al., 1999b) for typical marine boundary layer conditions.

The system is assumed to be in steady state prior to the perturbation, which is applied to $[O(^1D)]$ and allowed to propagate to perturb [OH] and $[HO_2]$. [NO] and $[NO_2]$

Table 1
Rate coefficients for linearized OH and HO_2 model system

Rate coefficient	10^{10}k(298 K)/cm^3 molecule s^{-1}	Reference
k_{1a}	2.20	DeMore et al. (1994)
k_{1b}	0.41	DeMore et al. (1994)
k_{1c}	0.26	DeMore et al. (1994)
k_2	0.00238	DeMore et al. (1994)
k_3	0.0849	Atkinson et al. (1992)
k_4	0.141	Atkinson et al. (1992)
k_5	0.0543	Atkinson et al. (1996)

Atmospheric number density $= 2.46 \times 10^{19}$ molecule cm^{-3}, $[O_3]_{fixed} = 30$ ppbv, $[CO]_{fixed} = 100$ ppbv, $[H_2O]_{fixed} = 1\%$ v/v; $O_3 \rightarrow O(^1D)$ photolysis rate coefficient $= 3.20 \times 10^{-5}$ s^{-1} representing mid-day, clear sky conditions and a solar zenith angle of 16° at a latitude of 40°.

are constrained to constant values so that the system is linear, except for the contribution from the $HO_2 + HO_2$ reaction, discussed below. The Jacobian for the three fast variables: $O(^1D)$, OH and HO_2 is shown in Eq. (15):

$$J = \begin{pmatrix} -k'_1 & 0 & 0 \\ 2\beta k'_1 & -(k'_2 + k'_4) & k'_3 \\ 0 & k'_2 & -(k'_3 + 4k'_5) \end{pmatrix}, \quad (15)$$

where $k'_n = k_n[x_i], [x_i]$ is a species whose concentration remains constant across the perturbation, $k'_1 = (k'_{1a} + k'_{1b} + k'_{1c})$ and $\beta = k'_{1a}/(k'_{1a} + k'_{1b} + k'_{1c})$. The Jacobian is only locally linear because of the inclusion of $[HO_2]$ in the Jacobian element, J_{33}; the factor of 4 arises from the differentiation of the peroxy–peroxy radical loss rate, $2k_5[HO_2]^2$, with respect to $[HO_2]$ to achieve local linearisation. HO_2 is formed from OH either directly (e.g. reaction R2) or, in more complex systems, via RO_2 and RO. Under most atmospheric conditions, the steady-state concentration of HO_2 exceeds that of OH by at least an order of magnitude. Since the perturbation is designed to change the concentration of OH only fractionally, the fractional change in $[HO_2]$ will be even smaller and the assumption of constant $[HO_2]$ throughout the relaxation following the perturbation is likely to be reasonable. The reciprocal chemical lifetimes are given by the absolute values of the diagonal elements, e.g. $1/\tau_{OH} = -J_{22} = (k'_2 + k'_4)$. The only off-diagonal element in the upper section of the matrix is k'_3 and the eigenvalue associated with the decay of $O(^1D)$ can be decoupled leaving a 2×2 matrix. The resulting determinant can be solved analytically as a quadratic equation to yield the eigenvalues given by

$$\lambda_{\pm} = -\tfrac{1}{2}(S \mp \sqrt{S^2 - 4Q}), \quad (16)$$

where

$$S = (k'_2 + k'_3 + k'_4 + 4k'_5), \quad (17)$$

$$Q = (k'_3k'_4 + 4k'_2k'_5 + 4k'_4k'_5). \quad (18)$$

We calculate the eigenvalues and chemical lifetimes for OH and HO_2 over a broad range of NO_x concentrations for $[NO_2]/[NO] = 0.1$ and $[NO_2]/[NO] = 5$ (Figs. 1 and 2). The NO and NO_2 concentrations drive much of the chemistry and the focus is on how the magnitude and the partitioning of NO_x between NO and NO_2 controls the coupling between OH and HO_2. The aim is to illustrate the effects of the interactions on the relaxation times rather than to simulate atmospheric conditions. Under more realistic tropospheric conditions, [NO] and $[NO_2]$ may change rapidly and such behaviour, which leads to a nonlinear system, is considered numerically in Section 6. In addition, the concentration ratio $[NO_2]/[NO] = 0.1$ is rarely established except, for example, for very short times in polluted conditions, such as, a power plant plume or polluted roadside conditions. This ratio was chosen to emphasise the effects of feedback from HO_2 to OH on the relaxation time/lifetime relationship.

At low [NO], for both sets of calculations, $(\tau_{OH})^{-1} \approx k_1[CO] \gg (\tau_{HO_2})^{-1} \approx 4k_5[HO_2]$. In consequence, $(\tau_{OH})^{-1} = -\lambda_-$ and $(\tau_{HO_2})^{-1} = -\lambda_+$ to a good approximation. The subsequent behaviour as [NO] increases depends on the $[NO_2]/[NO]$ ratio. As shown in Fig. 1, for $[NO_2]/[NO] = 0.1$ at high [NO], $(\tau_{HO_2})^{-1} > (\tau_{OH})^{-1}$, so there is a cross over in the relationship with the eigenvalues, and $(\tau_{OH})^{-1} \rightarrow -\lambda_+$, $(\tau_{HO_2})^{-1} \rightarrow -\lambda_-$. There are substantial deviations between $|\lambda_\pm|$ and reciprocal lifetimes at intermediate [NO]. As shown in Fig. 2, for $[NO_2]/[NO] = 5$, $(\tau_{OH})^{-1} > (\tau_{HO_2})^{-1}$ under all conditions and the eigenvalues can be identified primarily with one of the species. $|\lambda_-|$ tracks $(\tau_{OH})^{-1}$ and $|\lambda_+|$ tracks $(\tau_{HO_2})^{-1}$ closely, except for intermediate $[NO_x]$ where there is a significant deviation for both species where $|\lambda_-| > (\tau_{OH})^{-1}$ and $|\lambda_+| > (\tau_{HO_2})^{-1}$ so the radicals decay more quickly following a perturbation. The deviation appears more significant for $|\lambda_+|$ and $(\tau_{HO_2})^{-1}$ in Fig. 2 because of the logarithmic scale.

The origin of these qualitative relationships may be understood through examination of the analytic form of the eigenvalues. If $S^2 \gg 4Q$, then a binomial expansion of Eq. (16) gives

$$\lambda_+ \approx -\frac{Q}{S}, \quad (19)$$

$$\lambda_- \approx -S. \quad (20)$$

At low NO_x, for both $[NO_2]/[NO]$ ratios (since $k'_2 \gg 4k'_5$):

$$\lambda_+ \approx -\frac{(4k'_2k'_5)}{(k'_2 + 4k'_5)} \approx -4k'_5 = -(\tau_{HO_2})^{-1}, \quad (21)$$

$$\lambda_- \approx -(k'_2 + k'_4) = -(\tau_{OH})^{-1}. \quad (22)$$

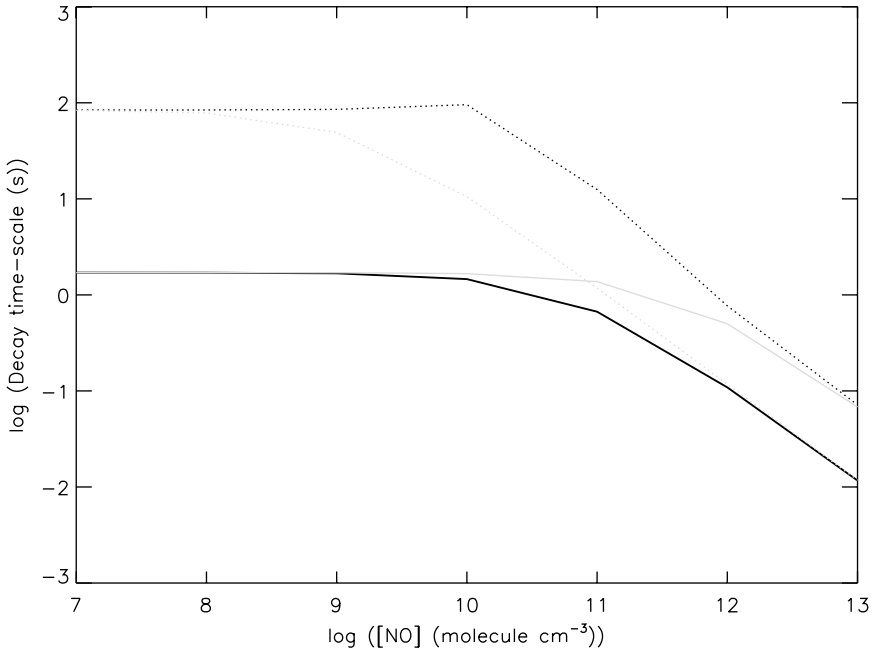

Fig. 1. Comparison of reciprocal eigenvalues and chemical lifetimes for linearized OH and HO_2 model system where $[NO_2]/[NO] = 0.1$. $\log(-1/\lambda_-)$ = black solid; $\log(-1/\lambda_+)$ = black dotted; $\log(\tau_{OH})$ = grey solid; $\log(\tau_{HO_2})$ = grey dotted.

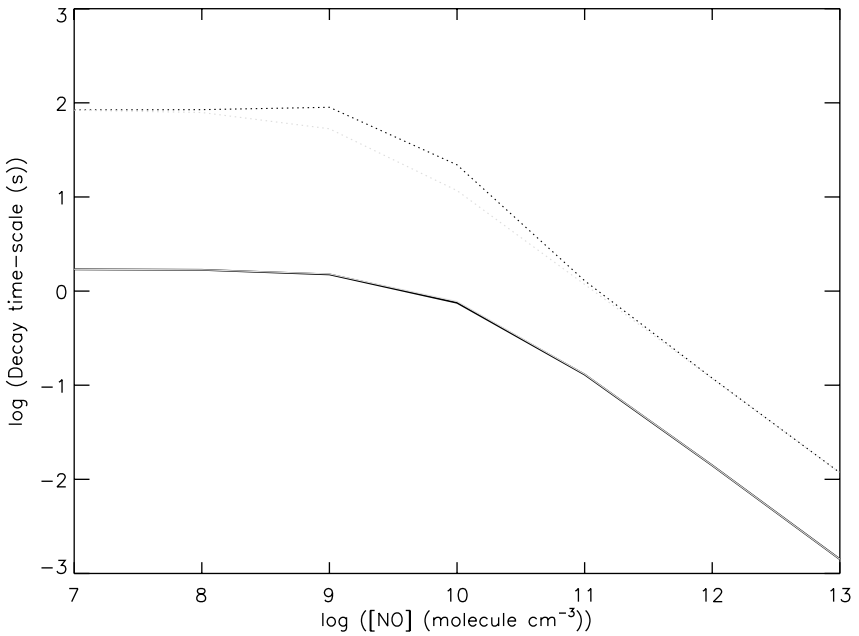

Fig. 2. Comparison of reciprocal eigenvalues and chemical lifetimes for linearized OH and HO_2 model system where $[NO_2]/[NO] = 5$. $\log(-1/\lambda_-)$ = black solid; $\log(-1/\lambda_+)$ = black dotted; $\log(\tau_{OH})$ = grey solid; $\log(\tau_{HO_2})$ = grey dotted. $\log(\tau_{OH})$ is underneath $\log(-1/\lambda_-)$.

At intermediate NO_x for $[NO_2]/[NO] = 5$

$$\lambda_+ \approx -k'_3 \frac{k'_4}{(k'_2 + k'_4)} \neq -(\tau_{HO_2})^{-1}, \tag{23}$$

$$\lambda_- \approx -(k'_2 + k'_3 + k'_4) \neq -(\tau_{OH})^{-1}. \tag{24}$$

In the case of λ_+, the absolute eigenvalue is equal to the inverse lifetime of HO_2 multiplied by a factor

representing the ratio of termination to termination + propagation.

At high NO_x, for $[NO_2]/[NO] = 5$ (since $k'_4 \gg k'_3$)

$$\lambda_+ \approx -\frac{(k'_3 k'_4)}{(k'_3 + k'_4)} \approx -k'_3 = -(\tau_{HO_2})^{-1}, \quad (25)$$

$$\lambda_- \approx -k'_4 = -(\tau_{OH})^{-1}, \quad (26)$$

for $[NO_2]/[NO] = 0.1$

$$\lambda_+ \approx -\frac{(k'_3 k'_4)}{(k'_3 + k'_4)} \approx -k'_4 = -(\tau_{OH})^{-1}, \quad (27)$$

$$\lambda_- \approx -(k'_2 + k'_3 + k'_4) \approx -k'_3 = (\tau_{HO_2})^{-1}. \quad (28)$$

The importance of the coupling term, k'_3, in the region where the eigenvalues and reciprocal lifetimes deviate for $[NO_2]/[NO] = 0.1$ at intermediate NO_x, is best illustrated by normalising with $(k'_2)^{-1}$ such that $\kappa_n = k'_n/k'_2$, $n = 1$–5. The reciprocal lifetimes of OH and HO_2 are given by $a = (1 + \kappa'_4)$ and $b = (\kappa'_3 + 4\kappa'_5)$, respectively. The approximate solutions for the eigenvalues become

$$|\lambda_+| \approx b - \frac{\kappa'_3}{a - b}, \quad (29)$$

$$|\lambda_-| \approx a + \frac{\kappa'_3}{a - b}. \quad (30)$$

The approximation is only valid when $\kappa'_3/(a - b)$ is small relative to a and b and the eigenvalues first start to separate. The extent of deviation of the eigenvalue solution from the reciprocal lifetime thus depends upon the feedback term, κ'_3 in the reaction matrix and also the separation of the lifetimes. For widely separated lifetimes, the second term tends to zero so there is no significant deviation from a or b. Thus, feedback from species with longer lifetimes only significantly affects the lifetime of a shorter-lived species if the coupling term is large and if the lifetimes are comparable. The form of Eqs. (29) and (30) and the nature of these conclusions derive directly from first-order perturbation theory (Atkins and Friedman, 1997).

5. Eigenvectors and contribution of species to eigenmodes

The elements of the transpose matrix of left eigenvectors, (u_{jk}^{-1}), characterise the contribution of the species to a given time-scale whilst the right eigenvector elements (u_{ij}) yield information about the contribution of a particular mode to species decay (Eq. (8)). The left eigenvector elements for the system have been calculated algebraically (Fig. 3). The elements are normalised to 1. In both regimes, at low NO_x, the decay of the fast time-scale species (OH) can be separated because $u_{jk}^{-1} = 1.0$.

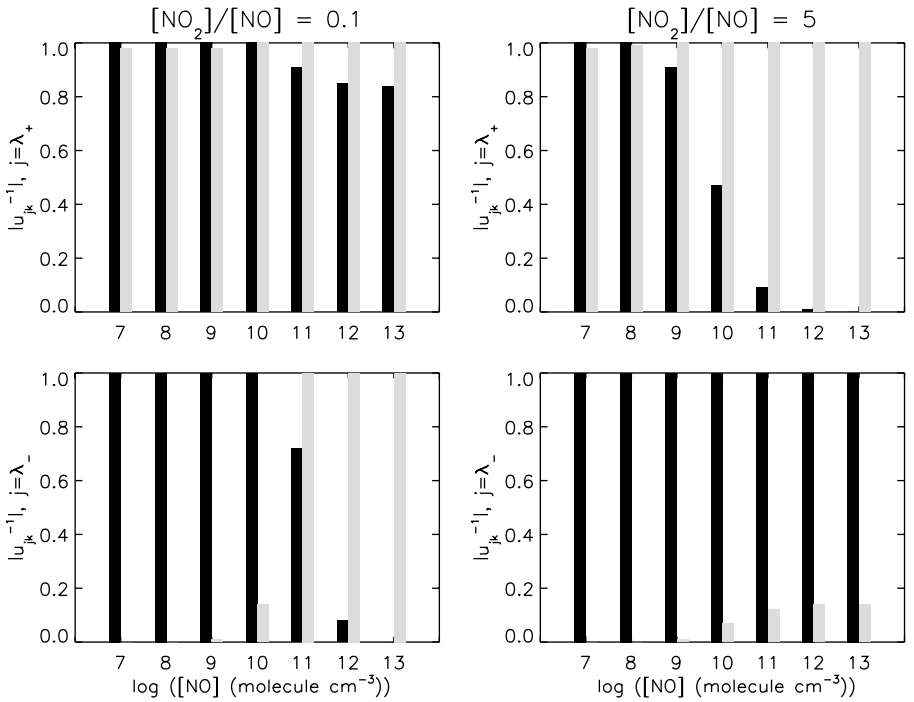

Fig. 3. Elements of the transpose of the left eigenvector matrix (u_{jk}^{-1}) for linearized OH and HO_2 model system. OH element = black shading; HO_2 element = grey shading.

Under these conditions, field measurement of the OH lifetime by a perturbation method provides the atmospheric lifetime as defined by Eq. (4). For $[NO_2]/[NO] = 0.1$ at high $[NO_x]$, the fast time-scale process can be separated out and attributed to the decay of HO_2 only. At $[NO] = 1 \times 10^{10}$–1×10^{11} molecule cm^{-3} there is strong coupling between the variables and the time-scales cannot be separated. Under low NO_x conditions in both NO_x regimes, there is strong coupling between OH and HO_2 in the slow decay mode (λ_+). The slow mode represents the slow loss of HO_x radicals from the system.

6. Atmospheric lifetimes of radicals in the marine boundary layer

The relationship between the coupling of chemical species and the chemical lifetimes and relaxation eigenvalues is examined with reference to field measurements made on the west coast of Ireland during the Eastern Atlantic Summer Experiment 1996 (EASE96) campaign, which was held at the remote coastal Mace Head Atmospheric Research station. The analysis of the field data, using detailed chemical models, has been discussed by Carslaw et al. (1999a, b) who constructed their chemical mechanism from an explicit master chemical mechanism (MCM) (Jenkin et al., 1997) based on the NMHCs measured during the campaign. The present analysis refers to 3rd August 1996, when concentrations of NMHC were very low, under clean westerly oceanic air flows. Carslaw et al. (1999b) reduced their chemical mechanism using an objective approach, based on sensitivity analysis. The simple form so obtained, includes an inorganic scheme and schemes for the oxidation of CO and CH_4 and is available on the World Wide Web (http://www.chem.leeds.ac.uk:80/Atmospheric/Field/model.html). The model was constrained to the measured concentrations of long-lived species (CO, CH_4, NO, NO_2, HCHO, and O_3) and meteorological parameters (temperature, water vapour, photolysis rates for O_3 and NO_2). The daily averaged concentrations were: $[CO] = 100$ ppbv (ppbv = parts per billion by volume), $[CH_4] = 1789$ ppbv, $[O_3] = 25$ ppbv, $[NO] = 21$ pptv (pptv = parts per trillion by volume) and $[NO_2] = 149$ pptv. Significant local perturbations to the NO and NO_2 concentrations were observed with spikes in $[NO_2]$ occurring at 06:00 h and 08:00 h when the concentration increased to 560 pptv and 1300 pptv, respectively, from the background value (149 pptv). A spike in [NO] also occurred at 08:00 h when the concentration increased to 549 pptv from the background value (21 pptv). The analysis in Sections 4 and 5 indicates that, for these conditions ($[NO_2]/[NO] = 7$, $[NO_2] = 1 \times 10^9$–3×10^{10} and $[NO] = 5 \times 10^8$–1×10^9), OH decays on a faster time-scale than HO_2 and that the OH decay time-scale is separable from HO_2 decay because $u_{jk}^{-1} = 1.0$.

The system can be described in terms of eight unconstrained species, $O(^1D)$, $O(^3P)$, CH_3O, OH, $CH_3O_2NO_2$, HO_2NO_2, CH_3O_2, HO_2, which have been ordered according to the increasing magnitude of their lifetimes. The eigenvalues and eigenvectors are calculated, based on the reduced mechanism, using a numerical method (http://www.nag.co.uk). There are eight real negative eigenvalue solutions, which encompass 13 orders of magnitude from, typically, -8×10^8 to -1×10^{-5} s^{-1}. The eigenvalue solutions are labelled λ_n in descending order of magnitude for $|\lambda_n|$. The diagonal Jacobian elements are defined as $J_{ii}(X)$ and encompass a narrower range of time-scales from -8×10^8 to -1×10^{-2} s^{-1}.

A comparison of the eigenvalues and diagonal Jacobian elements is shown in Table 2 for typical background daytime conditions (B) and across the NO_x perturbation (P) at 08:00 h. The diagonal Jacobian elements of the shortest lifetime radicals, $O(^1D)$, $O(^3P)$, CH_3O are indistinguishable from the "fastest" eigenvalues, λ_1, λ_2, λ_3, respectively. The diurnal variation of λ_4 and J_{ii}(OH) is shown in Fig. 4; the agreement is generally very good. Both are dominated by the terms in [CO] and [CH_4]; the large increase in magnitude at

Table 2
Comparison between eigenvalues (λ_i) and diagonal Jacobian elements (J_{ii}) for the marine boundary layer model. B denotes typical background conditions and P denotes [NO_x] perturbation

Mode i	Species	λ_i (s^{-1}) (B)	λ_i (s^{-1}) (P)	J_{ii} (s^{-1}) (B)	J_{ii} (s^{-1}) (P)
1	O^1D	-7.9358×10^8	-8.0209×10^8	-7.9358×10^8	-8.0209×10^8
2	O^3P	-7.9594×10^4	-8.0868×10^4	-7.9594×10^4	-8.0868×10^4
3	CH_3O	-8.5793×10^3	-8.6043×10^3	-8.5793×10^3	-8.6043×10^3
4	OH	-1.0889	-1.5178	-1.0860	-1.4555
5	$CH_3O_2NO_2$	-5.1840×10^{-1}	-6.5350×10^{-1}	-5.0149×10^{-1}	-4.7122×10^{-1}
6	HO_2NO_2	-3.4275×10^{-2}	-1.3456×10^{-1}	-2.7533×10^{-2}	-2.5817×10^{-2}
7	CH_3O_2	-6.1987×10^{-3}	-5.7797×10^{-2}	-2.0545×10^{-2}	-2.5550×10^{-1}
8	HO_2	-2.1147×10^{-3}	-9.4673×10^{-3}	-1.4315×10^{-2}	-1.6510×10^{-1}

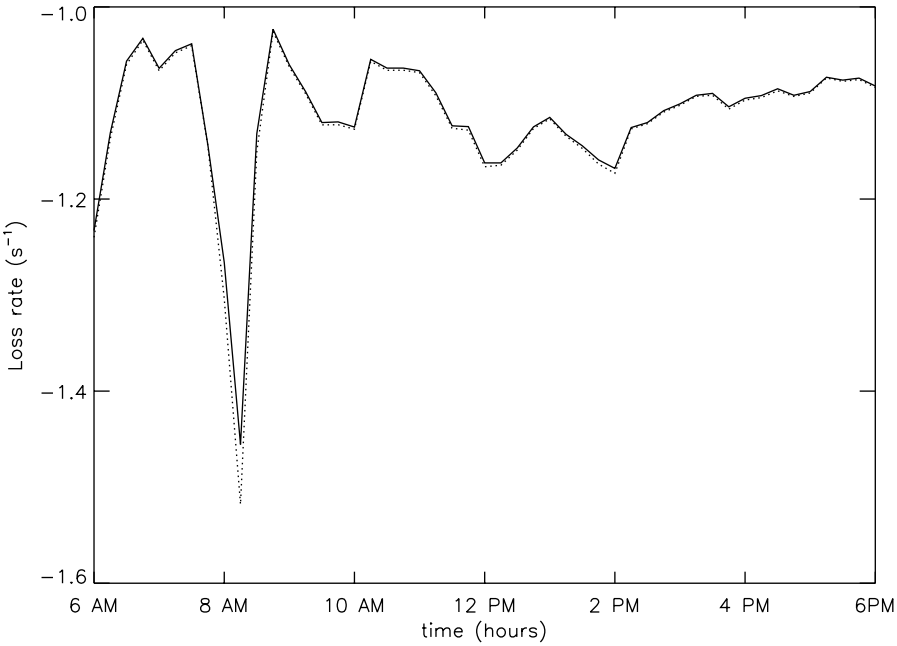

Fig. 4. Comparison of eigenvalue solution λ_4 and diagonal Jacobian element for OH on 3rd August 1996 at Mace Head, Ireland. J_{ii} (OH) = solid; λ_4 = dotted.

08.00 h arises because of an enhanced contribution from [NO_2]. However, there is a small difference between $|\lambda_4|$ and $|J_{ii}(OH)|$ which arises from increased coupling with HO_2 via NO. The time-scale separation between [OH] and [HO_2] drops from about 10^3 for background conditions to only about 10 during the perturbation. In general for the conditions experienced on 3rd August 1996 at Mace Head, the perturbation lifetime of OH is essentially equivalent to the atmospheric chemical lifetime as defined in Eq. (4).

The four "slow" eigenvalues, λ_5, λ_6, λ_7 λ_8, do not equate to the diagonal Jacobian elements of HO_2, CH_3O_2, HO_2NO_2 and $CH_3O_2NO_2$ (Table 2) and it is not possible to separate the time-scales for the decay of these species. The eigenvalue solutions, λ_5 to λ_8, span a range from about $-0.5\ s^{-1}$ to -1×10^{-3}. They are not related to simple sums of pseudo-first-order loss coefficients but are more complicated combinations thereof. The decay of each species occurs via a combination of some or all of the modes relating to eigenvalues λ_5 to λ_8 and a single eigenvalue solution represents the coupled decay of several species. Hence, there may be interference from several decay processes within each eigenvalue. λ_5 and λ_6 closely track $J_{ii}(CH_3O_2NO_2)$ and $J_{ii}(HO_2NO_2)$ for much of the day when background conditions are experienced and NO_x is very low. However, $|\lambda_5|$ and $|\lambda_6|$ increase in magnitude with increasing [NO_2]. Conversely, $J_{ii}(CH_3O_2NO_2)$ and $J_{ii}(HO_2NO_2)$ are unaffected by changes in [NO_2]. $|J_{ii}(CH_3O_2NO_2)|$ is between about 10 and 100 times larger than $|J_{ii}(HO_2)|$, $|J_{ii}(CH_3O_2)|$ and $|J_{ii}(HO_2NO_2)|$, which all have very similar inverse chemical lifetimes of the order of $1 \times 10^{-2}\ s^{-1}$.

Fig. 5 shows the diurnal variation of the "slow" eigenvalues λ_6–λ_8 and the diagonal Jacobian elements, $J_{ii}(HO_2NO_2)$, $J_{ii}(CH_3O_2)$ and $J_{ii}(HO_2)$. Throughout the day, the lifetime ordering (i.e. species are sorted according to increasing chemical lifetime) of HO_2, CH_3O_2, and HO_2NO_2 changes. $J_{ii}(HO_2NO_2)$ remains relatively constant throughout the whole day, whereas $J_{ii}(HO_2)$ and $J_{ii}(CH_3O_2)$ change significantly in response to the variations in [NO_2] and [NO]. For background conditions the ordering is $|J_{ii}(HO_2NO_2)| > |J_{ii}(CH_3O_2)| > |J_{ii}(HO_2)|$ whilst over the [NO_2] and [NO] perturbations the ordering changes $|J_{ii}(CH_3O_2)| > |J_{ii}(HO_2)| > |J_{ii}(HO_2NO_2)|$ or $|J_{ii}(HO_2)| > |J_{ii}(CH_3O_2)| > |J_{ii}(HO_2NO_2)|$ depending on the ratio [NO_2]/[NO].

The relaxation processes fused into a time-scale of the full system can be elucidated by inspection of the right and left eigenvector elements. The elements of the matrix of right eigenvectors (u_{ij}) and of the transpose matrix of left eigenvectors (u_{jk}^{-1}) for both typical background daytime conditions (B) and across the NO_x perturbation (P) are presented in Tables 3 and 4, respectively. The right eigenvector and left eigenvector solutions for λ_1, λ_2, λ_3 do not change with NO_x. However for λ_4, λ_5, λ_6, λ_7 and λ_8 there are significant changes to the dynamics across the NO_x perturbation.

The right eigenvector elements describe the contribution of each eigenmode to each species. The u_{ij} elements

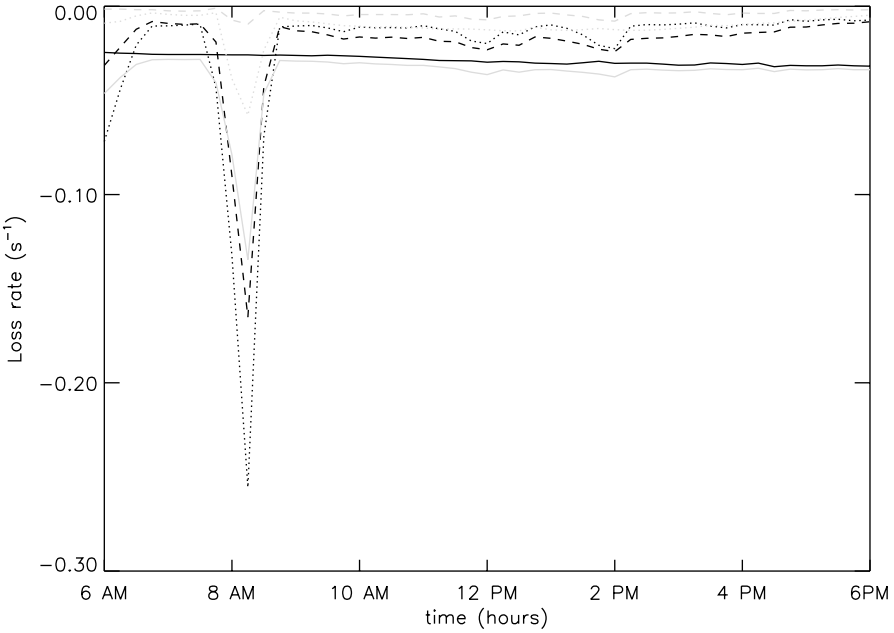

Fig. 5. Comparison of "slowest" eigenvalue solutions and diagonal Jacobian elements for "slowest" radicals HO_2NO_2, CH_3O_2 and HO_2, (which all have comparable lifetimes), on 3rd August 1996 at Mace Head, Ireland. λ_6 = grey solid; λ_7 = grey dotted; λ_8 = grey dashed; $J_{ii}(HO_2NO_2)$ = black solid; $J_{ii}(CH_3O_2)$ = black dotted; $J_{ii}(HO_2)$ = black dashed.

Table 3
Right eigenvector solutions (u_{ij}) for marine bounary layer model. B denotes typical background conditions and P denotes [NO_x] perturbation.

	j	λ_1	λ_2	λ_3	λ_4	λ_5	λ_6	λ_7	λ_8
i									
$O(^1D)$	B	0.74	0	0	0	0	0	0	0
$O(^3P)$	B	−0.68	1	0	0	0	0	0	0
CH_3O	B	0	0	0.71	0	0	0	0	0
OH	B	−0.16	0	0	0.81	0	0.01	0	0
	P	−0.16	0	0	0.87	0.02	−0.01	0.04	0.03
$CH_3O_2NO_2$	B	0	0	0	0	0.70	0	0	0.01
	P	0	0	0	0.03	0.63	0.09	0.15	0.02
HO_2NO_2	B	0	0	0	0	0	0.56	0.12	0.01
	P	0	0	0	0.02	0	0.38	−0.74	0.94
CH_3O_2	B	0	0	0	−0.18	−0.72	0.01	0.06	0.99
	P	0	0	0	−0.18	−0.76	0.21	0.40	0.07
HO_2	B	0	0	−0.71	−0.56	0	−0.86	0.99	0.01
	P	0	0	−0.71	−0.47	0.13	−0.89	0.51	0.33

for the λ_4 time-scale indicate that this mode contributes to the time dependence of the concentrations of OH ($u_{ij} \approx 0.8$) and also HO_2 ($u_{ij} \approx -0.6$) and CH_3O_2 ($u_{ij} \approx -0.2$), reflecting the decay pathways for OH on reaction with CO and CH_4 to yield HO_2 and CH_3O_2, respectively. The larger element for HO_2 arises because the rate of reaction with CO significantly exceeds that with CH_4 under Northern Hemispheric conditions. The species most affected by the decay on the λ_5 time-scale are CH_3O_2 ($u_{ij} \approx -0.7$) and $CH_3O_2NO_2$ ($u_{ij} \approx 0.7$). As [NO] increases, the HO_2 element increases ($u_{ij} \approx 0.1$) on the λ_5 time-scale. Decay on the λ_6 time-scale has the most significant effect on [HO_2] ($u_{ij} \approx -0.8$) and [HO_2NO_2] ($u_{ij} \approx 0.6$). The forward and reverse reaction rate coefficients are similar in magnitude for the observed NO_x field and so the relaxation time-scale encompasses reaction in both directions. The decay processes represented by λ_7 and λ_8 modes correspond to

Table 4
Left eigenvector transpose solutions (u_{jk}^{-1}) for marine bounary layer model. B denotes typical background conditions and P denotes [NO_x] perturbation

	k	$O(^1D)$	$O(^3P)$	CH_3O	OH	$CH_3O_2NO_2$	HO_2NO_2	CH_3O_2	HO_2
j									
λ_1	B	1	0	0	0	0	0	0	0
λ_2	B	0.67	0.75	0	0	0	0	0	0
λ_3	B	0	0	1	0	0	0	0	0
λ_4	B	0.21	0	0	1	0	0	0	0
	P	0.20	0	−0.04	0.98	0	0	0	−0.04
λ_5	B	0	0	0.01	−0.01	1	0	−0.04	0.01
	P	−0.02	0	0.02	−0.09	0.93	0	−0.36	0.02
λ_6	B	−0.02	0	−0.17	−0.11	0.05	0.91	0.04	−0.17
	P	-0.06	0	−0.43	−0.29	0.62	0.18	0.52	−0.43
λ_7	B	0.06	0	0.44	0.30	0.01	0.70	0.01	0.44
	P	0.04	0	0.15	0.19	0.71	0.12	0.63	0.15
λ_8	B	0.03	0	−0.04	0.13	0.70	−0.04	0.70	−0.04
	P	0.05	0	0.36	0.26	0.42	0.57	0.41	0.36

the leaking out of radicals from the system via radical–radical interactions on longer time scales than the interchange reactions between HO_2, HO_2NO_2 and OH.

The left eigenvector transpose elements give the contribution of each species to each different mode. $u_{jk}^{-1} = 1$ for $j = \lambda_4$ and $k = OH$, with the only other significant contribution deriving from $O(^1D)$, which has already collapsed on a time-scale of 10^{-8} s. Similarly $u_{jk}^{-1} = 1.0$, for $j = \lambda_5$ and $k = CH_3O_2NO_2$, with no other contributions under the unperturbed conditions, indicating that there is no coupling from other species on this time-scale. However, there is increased coupling across the [NO] perturbation at 08.00 h, while there is much greater coupling between the species for the slowest eigenvalues λ_6, λ_7 and λ_8. Particularly notable in the above examples is the formation of chemical "families", which have identical u_{jk}^{-1} elements within a mode, such as CH_3O and HO_2 in λ_6, λ_7 and λ_8 modes. "Families" denote a group of compounds having a large chemical exchange rate within the group, compared to the exchange with other chemical species (Shimazaki, 1984). Photochemical lifetimes for families are expected to be much longer than those for individual species of the family and family concentrations are usually more strongly affected by transport effects in the atmosphere.

7. Discussion

Model/measurement comparisons of [OH] in the boundary layer have frequently led to discrepancies of about 50%, with the model values exceeding those measured, as noted in the Introduction. Assessments of uncertainties in both sets of values indicate that this discrepancy is significant and its origin presumably lies in the neglect of species or of processes in the model. In relatively clean conditions, P (Eq. (2)) depends primarily on the rates of k_1' and on the rate of feedback from HO_2 to OH by reaction with NO and O_3. If [HO_2] is measured, then both these terms are relatively well defined. Any error is, therefore, likely to be found in the L term, which is equal to $(\tau_{OH})^{-1}$[OH]. In constrained box models, L is usually determined by measurement of all of the co-reactants for OH. In clean conditions, this is a relatively easy task, but it becomes much more difficult as pollution levels increase, especially given the results of Lewis et al. (2000) that indicate significant levels of 'undetected' hydrocarbons. Very recent results from a suburban campaign in Birmingham, UK (N. Carslaw, private communication) have shown that OH loss is dominated not by hydrocarbons but by oxygenates (alcohols and carbonyl compounds). Such species have been much more difficult to measure in the field, further compounding the problem of obtaining closure on L simply by measuring co-reactant concentrations. Lifetime measurements provide a powerful source of additional experimental information to effect this closure. The level of the observed discrepancy demonstrates that the experimental determination of τ_{OH} must be precise. Equally, it is essential that the measured relaxation time differs minimally from the OH lifetime. This paper has identified conditions where this equivalence is threatened, primarily from feedback from HO_2, where the lifetime of the peroxy radical approaches that of OH. However, for background tropospheric boundary layer conditions the dynamics of the tropospheric HO_x cycle results in significant time-scale separation ($(\tau_{OH})^{-1} \gg (\tau_{HO_2})^{-1}$) so that feedback via $HO_2 + NO$, is unlikely to reach a level sufficient to force a significant deviation between λ_i and $-(\tau_{OH})^{-1}$. The lifetime ordering is assured because the rate coefficient for $OH + NO_2$ is larger than that for $HO_2 + NO$, while under

steady-state boundary layer conditions $[NO]_2 > [NO]$. Furthermore, under polluted conditions where $[NO_x]$ is high, the concentration of hydrocarbons is expected to increase simultaneously with NO_x, thereby further decreasing the OH lifetime relative to that of HO_2.

The Mace Head experiments described in Section 6 show that OH lifetime measurement provides a satisfactory route to closure, while indicating that discrepancies could arise at higher $[NO_x]$. Except under clean conditions, it will always be advisable to carry out calculations to check for any nonequivalence.

Recently reported model/measurement comparisons for HO_2 at Mace Head (Carslaw et al., 2002) show much larger discrepancies and lifetime measurements for this species would be invaluable. The production term P is much more uncertain, since it depends strongly on carbonyl photolysis at even modest pollution levels while L depends on peroxy–peroxy reactions, in addition to reaction with NO and O_3. The former are difficult to quantify, especially under polluted conditions. These same reactions, however, also lead to strong coupling between several peroxy radicals, and to relaxation times that differ significantly from the chemical lifetimes. It is difficult to envisage a quantitative role for HO_2 lifetime measurements.

Previously, this type of analysis has been used to diagnose global perturbations to long-lived species (Prather, 1994, 1996, 1998) and perturbations to upper tropospheric photochemistry from deep convective injection of precursors (Jaegle et al., 2001). Here the response of radical species in simple tropospheric systems to small perturbations has been studied to investigate the relationship between atmospheric lifetime (τ^{-1}) and decay time (λ_i). The eigenvalues can be used to rigorously define modes of chemistry belonging to a certain time-scale. The modes are locally linear combinations of species concentrations that propagate synchronously in time on the same time-scale. From the experimental point of view, the modes can be used to study each relaxation time-scale.

In summary, the results suggest that assignment of a specific decay time to OH is appropriate for background tropospheric boundary layer conditions and therefore, that a lifetime field experiment would provide a clear measurement of the OH chemical lifetime. The results for the Mace Head system suggest that the coupling between peroxy species, through their cross reactions, is more complex, and that it is generally not possible to separate out species-specific time-scales for these species.

Acknowledgements

The authors thank Dr. S.H. Robertson for helpful discussions and NERC for funding and for a studentship for NB.

References

Arkin, A., Shen, P., Ross, J., 1997. A test case of correlation metric construction of a reaction pathway from measurements. Science 277, 1275–1279.

Atkins, P.W., Friedman, R.S., 1997. Molecular Quantum Mechanics. Oxford University Press, Oxford.

Atkinson, R., Baulch, D.L., Cox, A., Hampson, R.F., Kerr, J.A., Troe, J., 1992. Evaluated kinetic and photochemical data for atmospheric chemistry: supplement IV—IUPAC subcommittee on gas kinetic data evaluation for atmospheric chemistry. Journal of Physical Chemistry Ref. Data 21, 1125–1568.

Atkinson, R., Baulch, D.L., Cox, A., Hampson, R.F., Kerr, J.A., Rossi, M.J., Troe, J., 1996. Evaluated kinetic and photochemical data for atmospheric chemistry: supplement V. Atmospheric Environment 30, 3903–3904.

Atlas, E.L., Ridley, B.A., 1996. The Mauna Loa Observatory photochemistry experiment: introduction. Journal of Geophysical Research 101, 14531–14541.

Calpini, B., Jeanneret, F., Bourqui, M., Clappier, A., Vajtai, R., van den Bergh, H., 1999. Direct measurement of the total reaction rate of OH in the atmosphere. Analysis 27, 328–336.

Carslaw, N., Creasey, D.J., Heard, D.E., Lewis, A.C., McQuaid, J.B., Pilling, M.J., Monks, P.S., Bandy, B.J., Penkett, S.A., 1999a. Modelling OH, HO_2 and RO_2 radicals in the marine boundary layer: 1. Model construction and comparison with measurements. Journal of Geophysical Research 104, 30241–30255.

Carslaw, N., Jacobs, P.J., Pilling, M.J., 1999b. Modelling OH, HO_2 and RO_2 radicals in the marine boundary layer: 2. Mechanism reduction and uncertainty analysis. Journal of Geophysical Research 104, 30257–30273.

Carslaw, N., Creasey, D.J., Heard, D.E., Jacobs, P.J., Lee, J.D., Lewis, A.C., McQuaid, J.B., Pilling, M.J., Bauguitte, S., Penkett, S.A., Monks, P.S., Salisbury, G., 2002. Eastern Atlantic Spring Experiment 1997 (EASE97) 2. Comparison of model concentrations of OH, HO_2 and RO_2 with measurements. Journal of Geophysical Research 107 (D14) article number 4190.

Chameides, W.L., Perdue, E.M., 1997. Biogeochemical Cycles. Oxford University Press, Oxford.

Crosley, D.R., 1995. The measurement of OH and HO_2 in the atmosphere. Journal of Atmospheric Science 52, 3299–3314.

DeMore, W.B., Sander, S.P., Golden, D.M., Hampson, R.F., Kurylo, M.J., Howard, C.J., Ravishankara, A.R., Kolb, C.E., Molina, M.J., 1994. Chemical kinetics and photochemical data for use in stratospheric modeling. NASA Panel for Data Evaluation No. 10. Jet Propulsion Laboratory 94-26, JPL, Pasadena, CA, USA.

Eisele, F.L., Mount, G.H., Fehsenfeld, F.C., Harder, J., Madronich, E., Parrish, D.D., Roberts, J., Trainer, M.J., 1994. Intercomparison of tropospheric OH and ancillary trace gas measurements at Fritz Peak Observatory, Colorado. Geophysical Research Letters 99, 18605–18626.

Eisele, F.L., Tanner, D.J., Cantrell, C.A., Calvert, J.G., 1996. Measurements and steady state calculations of OH concentrations at mauna loa observatory. Journal of Geophysical Research 101, 14665–14679.

George, L.A., Hard, T.M., O'Brien, R.J., 1999. Measurement of free radicals OH and HO_2 in Los Angeles smog. Journal of Geophysical Research 104, 11643–11655.

Gray, P., Scott, S.K., 1991. Chemical Oscillations and Instabilities: Non-linear Chemical Kinetics. Oxford Science Publications, Oxford, UK.

Hard, T.M., O'Brien, R.J., Chan, C.Y., Mehrabzadeh, A.A., 1984. Tropospheric free radical determination by FAGE. Environmental Science and Technology 18, 768–777.

Hughes, K.J., Lightfoot, P.D., Pilling, M.J., 1992. Direct measurements of the peroxy–hydroperoxy radical isomerisation, a key step in hydrocarbon combustion. Chemical Physics Letters 191, 581–586.

Jaegle, L., Jacob, D.J., Brune, W.H., Wennberg, P.O., 2001. Chemistry of HO_x radicals in the upper troposphere. Atmospheric Environment 35, 469–489.

Jenkin, M.E., Saunders, S.M., Pilling, M.J., 1997. The tropospheric degradation of volatile organic compounds: a protocol for mechanism development. Atmospheric Environment 31, 81–104.

Kovacs, T.A., Brune, W.H., 1999. Total OH loss rate measurement. Eos Transactions 80, 46.

Lasaga, A.C., 1981. Dynamic treatment of geochemical cycles: global kinetics. Reviews in Mineralogy 8, 69–110.

Lasaga, A.C., Berner, R.A., 1998. Fundamental aspects of quantitative models for geochemical cycles. Chemical Geology 145, 161–175.

Lewis, A.C., Carslaw, N., Marriott, P.J., Kinghorn, R.M., Morrison, P., Lee, A.L., Bartle, K.D., Pilling, M.J, 2000. A larger pool of ozone-forming carbon compounds in urban atmospheres. Nature 405, 778–781.

McKeen, S.A., Liu, S.C., Mount, G., Eisele, F., Willams, E., Harder, J., Goldan, P., Kuster, W., Tanner, D., Fried, A., Sewell, S., Cantrell, C., Shetter, R., 1997. Photochemical modeling of hydroxyl and its relationship to other species during the tropospheric OH photochemistry experiment. Journal of Geophysical Research 102, 6467–6493.

Mount, G.H., Williams, E.J., 1997. An overview of the tropospheric OH photochemistry experiment Fritz Peak/Idaho Hill Colorado. Journal of Geophysical Research 102, 6171–6186.

Poppe, D., 1999. Time constant analysis of tropospheric gas-phase chemistry. Physical Chemistry and Chemical Physics 1, 5417–5422.

Prather, M.J., 1994. Lifetimes and eigenstates in atmospheric chemistry. Geophysical Research Letters 21, 801–804.

Prather, M.J., 1996. Natural modes and time scales in atmospheric chemistry: theory, GWPs for CH_4 and CO, and runaway growth. Geophysical Research Letters 23, 2597–2600.

Prather, M.J., 1998. Time scales in atmospheric chemistry: coupled perturbations to N_2O, NO_y, and O_3. Science 279, 1339–1341.

Shimazaki, T.J., 1984. The photochemical time constants of minor constituents and their families in the middle atmosphere. Atmospheric and Terrestrial Physics 46, 173–191.

Smith, G.P., Crosley, D.R., 1999. On direct measurements of atmospheric OH loss rates. Eos Transactions 80, 46.

Tomlin, A.S., Whitehouse, L., Lowe, R., Pilling, M.J., 2001. Low-dimensional manifolds in tropospheric chemical systems. Faraday Discussions 120, 125–146.

Turanyi, T., Tomlin, A.S., Pilling, M.J., 1993. On the error of the quasi-steady-state approximation. Journal of Physical Chemistry 97, 163–172.